Matrix Effects on Photoluminescence and Oxygen Sensitivity of a Molecular Ruby

Cui Wang[+],[a, c] Winald R. Kitzmann[+],[b] Florian Weigert,[a] Christoph Förster,[b] Xifan Wang,[a] Katja Heinze,*[b] and Ute Resch-Genger*[a]

The molecular ruby analogue $[Cr(ddpd)_2]^{3+}$ (ddpd = *N*,*N*′-dimethyl-*N*,*N*′-dipyridine-2-ylpyridine-2,6-diamine) exhibits near infrared (NIR) emission with a high photoluminescence (PL) quantum yield Φ_{PL} of 11 % and a lifetime of 898 μs in deaerated water at room temperature. While ligand-based control of the photophysical properties has received much attention, influences of the counter anions and microenvironment are still underexplored. In this study, the luminescence properties of the molecular ruby were systematically examined for the counter anions Cl^-, Br^-, $[BF_4]^-$, $[PF_6]^-$, $[BPh_4]^-$, and $[BArF_{24}]^-$ in acetonitrile (MeCN) solution, in crystals, and embedded into polystyrene nanoparticles (PSNP). Stern-Volmer analyses of the oxygen quenching studies in the intensity and lifetime domain showed the highest oxygen sensitivity of the complexes with the counter anions of $[BF_4]^-$ and $[BArF_{24}]^-$, which also revealed the longest luminescence lifetimes. Embedding $[Cr(ddpd)_2][PF_6]_3$ in PSNPs and shielding with poly(vinyl alcohol) yields a strongly NIR-emissive oxygen-insensitive material with a record Φ_{PL} of 15.2 % under ambient conditions.

Introduction

For decades, luminescent transition metal complexes have been in the focus of different research areas including photovoltaics,[1] bioimaging and biosensing,[2] photocatalysis,[3] and solid state lighting (active materials for organic light-emitting diodes (OLEDs)).[4] Until recently, such metal complexes solely relied on precious and rare-earth metals, *e.g.* platinum, ruthenium, iridium, or lanthanide ions.[5] Over the past years, growing efforts have been dedicated to develop and exploit new types of photoactive metal complexes based on earth-abundant metals, such as copper,[6] zirconium,[7] iron,[8] molybdenum,[9] manganese,[10] cobalt,[11] and chromium,[9d,12] which are considered as promising candidates for eco-friendly luminescence and photocatalysis applications.[13]

Amongst these coordination compounds, chromium(III) complexes have received much attention as near infrared (NIR) emitters.[12k,m,14] Previously, we reported an NIR-emissive ruby-analogue $[Cr(ddpd)_2]^{3+}$ (ddpd = *N*,*N*′-dimethyl-*N*,*N*′-dipyridine-2-ylpyridine-2,6-diamine) with a high photoluminescence (PL) quantum yield (Φ_{PL}) of 11 % and a long luminescence lifetime (τ_{PL}) of 898 μs in deaerated water at room temperature at the emission maximum of 778 nm (τ_{778}).[12b] Excitation of the complex at 435 nm from its $^4A_2$ ground state to the $^4T_2$ excited state, followed by rapid intersystem crossing (ISC) and vibrational cooling, leads to dual PL from the emissive doublet states $^2E/^2T_1$ at 738 and 775 nm. The luminescence of $[Cr(ddpd)_2]^{3+}$ responds to temperature,[12l] pressure[12e] and triplet oxygen,[12b] enabling a series of applications like multianalyte optical nanosensing,[12h] singlet oxygen generation for synthesis,[15] photodynamic therapy,[12c] circularly polarized luminescence,[16] and NIR-to-NIR upconversion in molecular chromium(III) ytterbium(III) salts at room temperature.[12i] In addition, by selective deuteration of the ddpd ligand, a Φ_{PL} of 30 % was observed, which presents a record value for an open-shell 3d metal complex in solution at room temperature.[12f]

A major advantage of the *Molecular Ruby* $[Cr(ddpd)_2]^{3+}$ over the solid-state material ruby is that the photophysical properties can be tuned by changing the first coordination sphere, *i.e.* the ligand.[12d,j,k,m,16b,c,17] For some cationic transition metal complexes, *e.g.* Ru^{II}, Cd^{II}, Yb^{III}, Ir^{III} or Cu^{I} complexes,[18] a strong effect on the photophysical properties was also found for their second coordination sphere. For instance, bulky counter ions could help to reduce the molecular aggregation of a cationic iridium(III) complex and reduce quenching pathways in crystalline solids, resulting in a 12-fold increase in Φ_{PL}.[19] In our recently reported second-generation *Molecular Ruby* $[Cr(bpmp)_2]^{3+}$ (bpmp = 2,6-bis(2-pyridylmethyl)pyridine), the second coordination sphere, *i.e.* counter anions and solvent

[a] *Dr. C. Wang,[+] Dr. F. Weigert, X. Wang, Dr. U. Resch-Genger*
Division Biophotonics
Federal Institute for Materials Research and Testing (BAM)
Richard-Willstätter-Straße 11, 12489 Berlin (Germany)
E-mail: ute.resch@bam.de
[b] *W. R. Kitzmann,[+] Dr. C. Förster, Prof. Dr. K. Heinze*
Department of Chemistry
Johannes Gutenberg University of Mainz
Duesbergweg 10–14
55128 Mainz (Germany)
E-mail: katja.heinze@uni-mainz.de
[c] *Dr. C. Wang[+]*
Institute of Chemistry and Biochemistry
Free University of Berlin
Arnimallee 22, 14195 Berlin (Germany)
[+] *These authors contributed equally to this work.*

Supporting information for this article is available on the WWW under https://doi.org/10.1002/cptc.202100296

molecules, interacts with the chromium(III) ion via the ligands' acidic methylene bridges, thereby affecting its Φ_{PL} values and PL lifetimes.[12k] Conductivity measurements of $[Cr(ddpd)_2][BF_4]_3$ (**CrBF$_4$**) in acetonitrile revealed that on average a contact ion pair of one complex cation and one $[BF_4]^-$ anion prevails, which suggests a strong interaction between the triply charged cation and the counter anions.[12c] This observation inspired us to explore the untapped potential of the tuning of the optical properties and photophysics of $[Cr(ddpd)_2]^{3+}$ by the choice of the counter anion and encouraged us to systematically study the influence of six counter anions of varying bulkiness on Φ_{PL}, τ_{PL}, and the O_2 sensitivity of the resulting $[Cr(ddpd)_2]^{3+}$ complexes in crystalline solids, acetonitrile (MeCN) solution, and encapsulated in 100 nm aminated polystyrene nanoparticles (PSNP). Our study covers $[Cr(ddpd)_2]^{3+}$ salts with the halide counter anions chloride Cl^- (**CrCl**) and bromide Br^- (**CrBr**), tetrafluoroborate $[BF_4]^-$ (**CrBF$_4$**), hexafluorophosphate $[PF_6]^-$ (**CrPF$_6$**), tetraphenyl borate $[BPh_4]^-$ (**CrBPh$_4$**), and tetrakis[3,5-bis(trifluoromethyl)phenyl]borate $[BArF_{24}]^-$ (**CrBArF$_{24}$**) (Scheme 1).

Results and Discussion

Synthesis, Crystal Structures, and PSNP Encapsulation of $[Cr(ddpd)_2][X]_3$

The known ligand ddpd was prepared in a 33 g scale reaction according to a modified literature procedure (for details see Supporting Information (SI)).[20] The crude product was purified by precipitation of $[H_2ddpd][BF_4]_2$ using $HBF_4{\cdot}Et_2O$ and subsequent recrystallization, thereby elegantly circumventing column chromatography. Deprotonation with aqueous sodium hydroxide solution and extraction yielded pure ddpd in a high yield of 75%. The chromium(III) salts **CrBF$_4$**, **CrPF$_6$** and **CrBPh$_4$** were synthesized according to literature procedures.[12b,h] The salts **CrCl**, **CrBr** and **CrBArF$_{24}$** were obtained from **CrBF$_4$** via counter-ion exchange (see Supporting Information). An alternative method for the preparation of **CrCl** utilized $CrCl_2$, ddpd and NH_4Cl (route A, see SI for details).

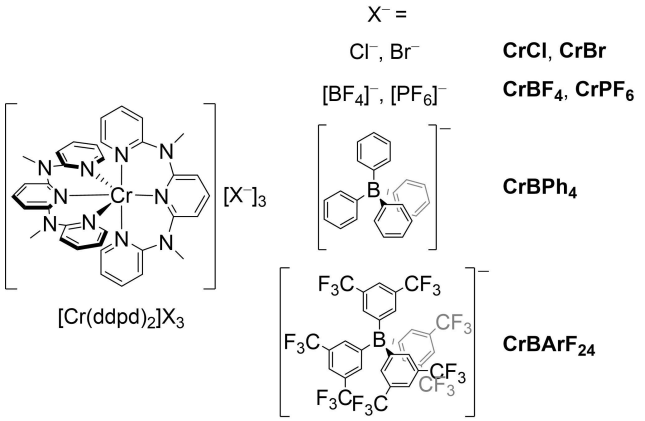

Scheme 1. Chemical structure of $[Cr(ddpd)_2]^{3+}$ with various counter anions.

Single crystals of **CrCl**, **CrBr**, **CrBF$_4$**, and **CrPF$_6$** suited for X-ray diffraction analysis were grown by diffusion of diethyl ether in concentrated solutions in MeCN, d_3-MeCN, MeOH or EtOH (see the Supporting Information for details).[39] The crystal structures were determined by X-ray crystallography (Table 1; SI, Table S1). NH_4Cl, which co-crystallized in **CrCl-A**, stems from the synthesis of **CrCl** via the $CrCl_2/NH_4Cl$ preparation (route A).

Crystallization of **CrCl** from MeOH and EtOH gave rise to a variety of pseudo-polymorphs differing in number and type of co-crystallized solvent molecules (**CrCl-A**–**CrCl-D**). These results underline the flexibility of the crystal packings containing a highly charged cation like $[Cr(ddpd)_2]^{3+}$ in combination with small counter anions. **CrBr** crystallized from MeCN under ambient conditions as **CrBr**×3 H_2O×MeCN (**CrBr-A**). Single crystals of literature known **CrBF$_4$**×3 MeCN (**CrBF$_4$-A**),[12b] which are several millimeter in length, were reproducibly obtained through the diffusion of diethyl ether in a complex solution in MeCN/H_2O (v/v, 100/1) (SI, Figure S1). To investigate the effect of solvent deuteration in the solid state, **CrBF$_4$** was crystallized from d_3-MeCN yielding the same structure (sample denoted as **[D$_9$]-CrBF$_4$-A**). In our crystallization attempts, **CrPF$_6$** formed crystals containing three equivalents of MeCN, instead of two as in the previously reported pseudo-polymorphs.[12b]

All Cr–N bond lengths lie in the range of 2.017–2.060 Å and the N–Cr–N angles are in the ranges of 84–97° and 171–180° (SI, Figures S2 and S3), respectively, revealing the nearly ideal octahedral geometry of $[Cr(ddpd)_2]^{3+}$. Thus, the counter anions and the co-crystallized solvent molecules and salts barely influence the structure of the complex cation. The distances between the chromium(III) centers and the nearest counter ions range from d(Cr···F) = 4.424(4) Å) (**CrBF$_4$-A**) to d(Cr···Cl) = 5.7160(17) Å (**CrCl-A**) (Table 1). The shortest Cr···Cr distances range from 9.2 to 10.5 Å (Table 1) (discussion see below).

The complexes **CrBF$_4$**, **CrPF$_6$**, **CrBPh$_4$**, and **CrBArF$_{24}$** were encapsulated into 100 nm-sized aminated PSNPs via a simple one-step staining procedure (SI, Scheme S1) developed for hydrophobic compounds.[21] This loading procedure is not feasible for the hydrophilic complexes **CrCl** and **CrBr** and apolar PSNP. To avoid complex leaking, a thin silica shell with a thickness of about 5–7 nm was coated on the surface of the particles via an ammonia-catalyzed Stöber process,[12h,22] yielding silanized **PS(Cr)-S** particles which are water dispersible. The

Table 1. Composition and space group of the crystals of $[Cr(ddpd)_2]^{3+}$ with different counter-ions with the shortest Cr···Cr distances d(Cr···Cr) and shortest Cr···counter-ion distances d(Cr···X) (X=F/Cl/Br) listed.[a]

Crystals	Composition	d(Cr···Cr) [Å]	d(Cr···X) [Å]
CrCl-A	**CrCl**×3.5 MeOH, ×0.5 NH_4Cl	10.106(2)	5.7160(17)
CrCl-B	**CrCl**×3 EtOH, ×H_2O	9.705(2)	4.730(7)
CrCl-C	**CrCl**×2 MeOH, ×4 H_2O	9.825(2)	4.8383(17)
CrCl-D	**CrCl**×2 EtOH, ×3 H_2O	9.502(2)	4.9351(16)
CrBr-A	**CrBr**×3 H_2O, ×MeCN	9.8173(19)	4.953(1)
CrBF$_4$-A	**CrBF$_4$**×3 MeCN	10.458(2)	4.424(4)
[D$_9$]-CrBF$_4$-A	**CrBF$_4$**×3 d_3-MeCN	10.458(2)	4.424(4)
CrPF$_6$-A	**CrPF$_6$**×3 MeCN	9.198(2)	4.594(3)

[a] Note: Co-crystallized molecules are indicated with an "×". The standard deviations of the distances are given in brackets.

complexes with the bulky counter anions **$CrBPh_4$** and **$CrBArF_{24}$** show a higher loading capacity due to their more pronounced hydrophobicity than the water-soluble salts **$CrBF_4$** and **$CrPF_6$**.[12h] Additionally, the **PS(Cr)-S** particles were mixed with an oxygen-barrier polymer poly(vinyl alcohol) (PVOH) and dried under reduced pressure, resulting in a polymeric film **PS(Cr)-S-PVOH** (see SI for details).

Luminescence Properties of Crystals of CrCl, CrBr, $CrBF_4$, and $CrPF_6$

Emission spectra of crystalline **CrCl-A**, **CrCl-B**, **CrBr-A**, **$CrBF_4$-A**, **[D_9]-$CrBF_4$-A** and **$CrPF_6$-A** suspended in paraffin oil were recorded on a microscope setup using excitation at 405 nm under ambient conditions (SI, Figures S4–S15, Tables S2–S7). Exemplary microscopy and PL images of **$CrBF_4$-A** crystals are depicted in Figure 1c. Several crystals of each sample were excited with the 405 nm laser and the resulting PL was measured at different positions of the crystals. This gave two strong emission bands peaking at 738–745 nm and 775–783 nm ($^2T_1 \rightarrow {}^4A_2$ and $^2E \rightarrow {}^4A_2$, Figures 1a; SI, Figures S5, S7, S10, S11, S13, S15), in accordance with measurements of $[Cr(ddpd)_2]^{3+}$ in solution (see below and ref. [12b]). A slight redshift of the emission bands was observed in some cases (SI, Figures S5, S7, S10, S11, S13, and S15). This is tentatively attributed to small local changes of the complex geometry due to defects. The intensity ratios of the two emission bands were not constant during the PL experiments (Figure 1a). An earlier study showed that the two emissive states $^2T_1$ and ^2E are in thermal equilibrium.[12l] This suggests that these effects arise from different local temperatures due to heating by the focused excitation light. With the established intensity ratio relationship of the two emission bands,[12l] a temperature difference of ca. 40 K can be estimated for example between spot 4 and spot 5 (Figure 1a).

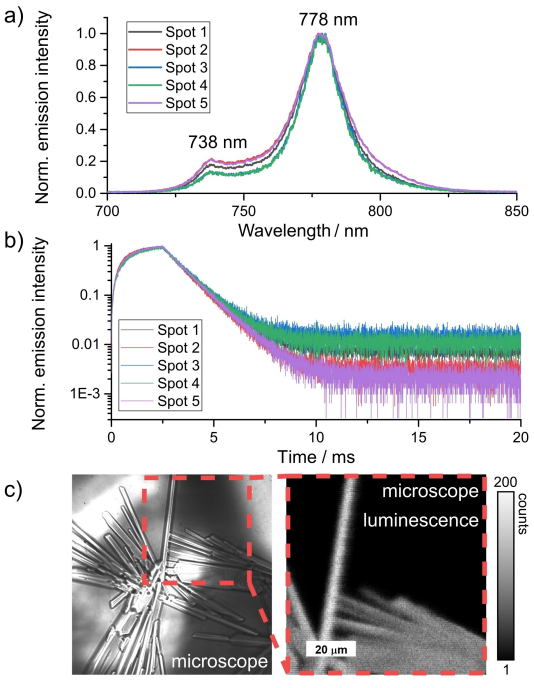

Figure 1. a) Normalized luminescence emission spectra, b) PL decays (detection range 600–1000 nm; 2.5 ms excitation duration), and c) exemplary microscopy (left) and PL image of the marked area (right, $\lambda_{exc} = 405$ nm, $\lambda_{em} = 600$–1000 nm) of crystals of **$CrBF_4$-A**. Excitation was done with a 405 nm laser. The scale bar is 20 µm. All measurements were performed under ambient conditions.

Luminescence lifetimes were determined from PL decay measurements performed with the same microscope by exciting the sample with a 405 nm laser with a focused laser spot repeatedly for a duration of 2.5 ms and recording the PL signal in the spectral window of 600–1000 nm (Figure 1b; SI, Figures S5, S8, S10, S11, S13, S15) within a time window of 17.5 ms. During recording the PL signal, the laser was switched off. Laser excitation led to an increasing population of the excited states[23] during the 2.5 ms-long period of laser excitation, followed by the radiative depopulation of these emissive levels. The obtained luminescence decays could be well reproduced with a biexponential fit, yielding a long- and a short-lived decay component (τ_{long} and τ_{short}). Exceptions are all decays of **$CrBF_4$-A** and three decays of **CrCl-A**, where a mono-exponential fit was sufficient (SI, Tables S2–S7). While the longer lifetime originates from the radiative depopulation of the emissive doublet states $^2E/^2T_1$, the short-lived component most likely arises from excited complexes formed by doublet-doublet energy transfer between the chromium(III) complexes inside the crystal to trap states with slightly lower $^2E/^2T_1$ energies. This assumption is supported by the shortest Cr···Cr distances of 9.2–10.5 Å (Table 1), which is close to the limit of Dexter-type energy transfer between chromium(III) complexes.[24] Additional luminescence studies of the exemplary chosen water-insoluble **$CrBPh_4$** salt in MeCN/H_2O solvent mixtures of varying water content revealed the water-induced formation of aggregates. Upon aggregation, in the presence of large amount of water (70–99 vol%), the luminescence decay kinetics of **$CrBPh_4$** which are monoexponential in MeCN, became biexponential (SI, Figure S16 and Table S8). Aggregation of **$CrBPh_4$** results in a shortening of the intermolecular distances between the complexes and allows for energy transfer between the chromium(III) centers. This accounts for the observed shorter lifetimes and supports our assumption of a distance-dependent doublet-doublet energy transfer between the chromium(III) centers in the crystals. Energy migration between chromium(III) complexes has been observed in solution and in the solid state before.[14g,25] For example, in $Na[Ru(bpy)_3][Cr(ox)_3]$ (bpy = 2,2′-bipyridine, ox^{2-} = oxalate^{2-}), the excitation energy is transferred from excited $[Cr(ox)_3]^{3-}$ moieties in the bulk to ground state molecules near the microcrystal surface.[25] For $[Cr(ddpd)_2]^{3+}$, the Φ_{PL} values, which were determined absolutely using an integrating-sphere setup, the fitted lifetimes ($<\tau_{long}>$ and $<\tau_{short}>$ with their relative amplitudes), and the averaged amplitude-weighted lifetimes of all crystals are summarized in Table 2 and illustrated in Figure 2.

The crystals of **[D_9]-$CrBF_4$-A** grown from deuterated and non-deuterated MeCN show similar $<\tau_{long}>$ and Φ_{PL} (Table 2).

Table 2. Luminescence properties of $[Cr(ddpd)_2]^{3+}$ in different salts varying in counter anion and crystal environments including the averaged lifetimes $<\tau_{long}>$ and $<\tau_{short}>$ (averaged relative amplitudes given in brackets), the average of the amplitude weighted lifetimes $<\tau_{avg}>$, and quantum yield Φ_{PL}.[a]

Crystals	$<\tau_{long}>$ [μs]	$<\tau_{short}>$ [μs]	$<\tau_{avg}>$ [μs]	Φ_{PL} [%]
$CrBF_4$-A	1026 ± 36		1026 ± 36	13.8 ± 0.3
[D_9]-$CrBF_4$-A	1062 ± 42 (0.71)	620 ± 100 (0.29)	947 ± 65	14.1 ± 0.5
$CrPF_6$-A	916 ± 133 (0.58)	529 ± 136 (0.42)	754 ± 128	10.1 ± 0.7
CrCl-A	853 ± 73 (0.63)	469 ± 52 (0.37)	728 ± 122	10.8 ± 0.2
CrCl-B	889 ± 203 (0.50)	417 ± 179 (0.50)	663 ± 214	11.2 ± 0.2
CrBr-A	394 ± 94 (0.45)	193 ± 63 (0.55)	288 ± 98	4.5 ± 0.2

[a] For lifetime measurements: λ_{exc} = 405 nm, λ_{em} = 600–1000 nm; for quantum yield measurements: λ_{exc} = 435 nm. All data were obtained under ambient conditions. The standard errors of Φ_{PL} shown in the table are derived from at least ten repetitive measurements of each sample under identical conditions. The standard errors of τ shown in the table are obtained from at least eight measurements under identical conditions on various spots of each crystalline sample.

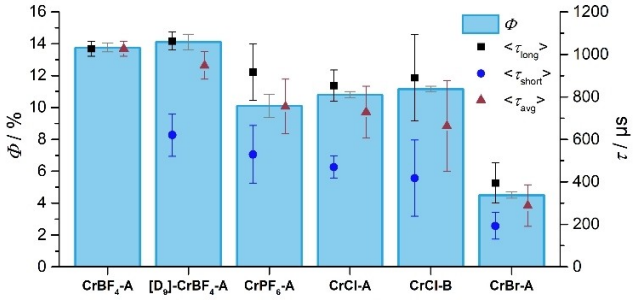

Figure 2. Luminescence properties of $[Cr(ddpd)_2]^{3+}$ in different crystal packings with the separately averaged long and short lifetime components $<\tau_{long}>$ and $<\tau_{short}>$, the average of the amplitude averaged lifetimes $<\tau_{avg}>$, and the PL quantum yields Φ_{PL}. For lifetime measurements: λ_{exc} = 405 nm, λ_{em} = 600–1000 nm; for quantum yield measurements: λ_{exc} = 435 nm. All data were obtained under ambient conditions and shown with their error bars.

Also measurements in MeCN and d_3-MeCN solutions revealed matching results.[12f] These findings suggest that the second sphere deuteration has only a marginal effect on the non-radiative decay pathways in the crystal and in acetonitrile solution. In contrast to **$CrBF_4$-A** and **[D_9]-$CrBF_4$-A**, the crystals **CrCl-A**, **CrCl-B**, **CrBr-A**, and **$CrPF_6$-A** exhibited a broader distribution of luminescence lifetimes. This possibly reflects a more heterogeneous crystal size distribution of these samples containing overall smaller crystals. PL lifetimes and Φ_{PL} of **CrCl-A**, **CrCl-B**, and **$CrPF_6$-A** are similar with values between 850–950 μs and 10–11 % (Figure 2). This suggests only a minor effect of the environment and the counter anion on their optical properties.

However, a strong influence of the solid state was found for **CrBr-A**. In this bromide salt, Φ_{PL} and $<\tau_{long}>$ are significantly reduced to 4.5 ± 0.2 % and 394 ± 94 μs. In principle, photo-induced electron transfer (PET)[26] from Br^- to excited $^2[Cr(ddpd)_2]^{3+}$ yielding $Br^\bullet$ and $[Cr(ddpd)_2]^{2+}$ is conceivable with the short Cr···Br distance of 4.953(1) Å in the crystal. This PET process is thermodynamically unfavorable with $E_{1/2}$*([Cr(ddpd)$_2$]$^{3+/2+}$) = 0.49 V in MeCN[12b] and $E_{1/2}(Br^\bullet/Br^-)$ = 1.28 V/0.82 V (versus ferrocene/ferrocenium) in water and acetone, respectively.[26b,27] In deaerated MeCN solution, **CrBr** did not show a comparable reduction of Φ_{PL} and lifetime (Φ_{PL} = 9.8 ± 0.5 %, τ_{778} = 806 ± 40 μs, Table 3). However, the redox potentials in the crystal lattice are unknown and hence, PET in the solid state could be downhill in the specific environment of the **CrBr-A** crystal. The bromide ions in **CrBr-A** are hydrogen-bonded to crystal water and the shortest Br···Br distance amounts to 6.2128(13) Å. An alternative explanation for the observed PL quenching could be the large spin-orbit coupling constant of bromide that could accelerate non-radiative and radiative decay processes to the ground state via ISC in the crystal lattice.[28] This phenomenon is known as external heavy-atom effect and has been used to enhance room temperature phosphorescence of organic dyes.[28] In-depths mechanistic investigations of the luminescence quenching mechanisms of $[Cr(ddpd)_2]^{3+}$ via an external heavy atom effect, PET or a

Table 3. Φ_{PL} and τ_{778} (with relative amplitude in brackets) data of $[Cr(ddpd)_2]^{3+}$ with various counter anions in MeCN solution, in PSNP, and in PSNP sealed in an oxygen-barrier PVOH film.[a]

	MeCN solution		PS(Cr)-S		PS(Cr)-S-PVOH
	Φ_{air} [%] (τ_{air} [μs])	Φ_{Ar} [%] (τ_{Ar} [μs])	Φ_{air} [%] (τ_{air} [μs])	Φ_{Ar} [%] (τ_{Ar} [μs])	Φ_{air} [%](τ_{air} [μs])
CrCl	0.6 ± 0.1 (48 ± 2)	5.2 ± 0.3 (472 ± 24)			
CrBr	0.9 ± 0.1 (52 ± 3)	9.8 ± 0.5 (806 ± 40)			
$CrBF_4$	0.8 ± 0.1[b] (52 ± 3)	13.7 ± 0.7 (1122 ± 56)	3.6 ± 02 (277 ± 14)	10.0 ± 0.5 (885 ± 44)	11.7 ± 0.6 (τ_{long}: 930 ± 47 (0.94); τ_{short}: 330 ± 17)
$CrPF_6$	0.8 ± 0.1[b] (52 ± 3)	11.7 ± 0.6[b] (900 ± 45)	2.9 ± 0.1 (241 ± 12)	10.3 ± 0.5 (928 ± 46)	15.2 ± 0.8 (τ_{long}: 980 ± 49 (0.92); τ_{short}: 360 ± 18)
$CrBPh_4$	0.7 ± 0.1 (45 ± 2)	9.2 ± 0.5 (780 ± 39)	2.7 ± 0.1 (254 ± 13)	6.4 ± 0.3 (686 ± 34)	11.3 ± 0.6 (τ_{long}: 980 ± 49 (0.90); τ_{short}: 460 ± 23)
$CrBArF_{24}$	1.0 ± 0.1 (52 ± 3)	13.6 ± 0.7 (1112 ± 56)	1.7 ± 0.1 (τ_{long}: 280 ± 14 (0.61); τ_{short}: 66 ± 3)	14.4 ± 0.7 (1200 ± 60)	13.4 ± 0.7 (τ_{long}: 960 ± 48 (0.90); τ_{short}: 410 ± 21)

[a] PS(Cr)-S: PSNPs doped with chromium(III) complexes and coated with silica shell; PS(Cr)-S-PVOH: PS(Cr)-S particles sealed in PVOH film. Measurements were done with λ_{exc} = 435 nm and λ_{em} = 778 nm. The standard errors of Φ_{PL} shown in the table are derived from at least ten repetitive measurements of each sample under identical conditions. The errors of τ_{778} are estimated with a relative uncertainty of 5 %. [b] Φ_{PL} and τ_{778} are cited from ref. [12b].

combination of both processes are beyond the scope of this study.

Overall, Φ_{PL} and $<\tau_{long}>$ are affected by changes in the complex environment in the crystal structures. The observed parallel trends for both quantities (Figure 2) suggest that only the emissive doublet states are influenced by the second coordination sphere. In contrast, ISC from the initially excited $^4T_2$ levels to the doublet manifold (3.5 ps in solution)[15] is barely affected, because otherwise the PL quantum yield should change, while the lifetime of the doublet state is expected to remain constant. In our case, the observed strong correlation between Φ_{PL} and $<\tau_{long}>$ suggest that the counter anions and the microenvironment only influence the radiative and non-radiative relaxation pathways from the emissive doublet states to the ground state of the chromium complexes.

Luminescence Properties of $[Cr(ddpd)_2][X]_3$ in Acetonitrile Solution

All luminescence experiments were performed in MeCN due to the good solubility of all six complex salts in this solvent. All six compounds show identical absorption and emission spectra in MeCN (Figure 3a), indicating that the energy levels of the involved electronic states are unaffected by the counter anion X^- despite the formation of contact ion pairs in solution.[12c] A comparison of complexes **CrCl**, **CrBr**, **$CrPF_6$**, and **$CrBArF_{24}$** reveals an enhancement of the PL with increasing bulkiness of the anions (Figure 3b–c). Φ_{PL} and τ_{778} of the bulkiest complex salt **$CrBArF_{24}$** amount to 13.6 ± 0.7 % and 1112 ± 56 µs, respectively. This presents an enhancement by a factor of ca. 2.5 compared to the chromium(III) complex with the smallest anion of this series, here **CrCl** showing a Φ_{PL} value of 5.2 ± 0.3 %, and a τ_{778} of 472 ± 24 µs in MeCN (Table 3). This is attributed to a steric shielding effect of the counter anion, which can partially hamper non-radiative decay pathways caused by intermolecular interactions.[19] The lower Φ_{PL} and τ_{778} values of the **CrCl** salt are attributed to self-quenching caused by chloride anions, which can act as bridges between the complex cations.[14g,29] This was confirmed by Stern-Volmer studies with **CrCl** and tetrabutylammonium chloride (TBAC) which revealed the occurrence of static quenching at high Cl^- concentrations (SI, Figure S30).

Interestingly, new measurements of **$CrBF_4$** in thoroughly degassed MeCN reveal a lifetime (1122 ± 56 µs) and quantum yield (13.7 ± 0.7 %) comparable to **$CrBArF_{24}$**. This 25 % increase with regards to previously reported values[12b] can be explained by small traces of dioxygen which were present in earlier measurements and which can quench the long-lived excited states of $[Cr(ddpd)_2]^{3+}$ very efficiently (see below). The consistently higher lifetime and quantum yield of **$CrBF_4$** compared to **CrCl**, **CrBr** and **$CrPF_6$** in MeCN and in single crystals (Tables 2 and 3) cannot be explained with the bulkiness of the counter anions, which suggests that an unknown additional factor may be at play for this salt.

The smaller Φ_{PL} and a shorter τ_{778} of **$CrBPh_4$** compared to **$CrBF_4$** (Figure 3c) is ascribed to π-π and CH–π stacking

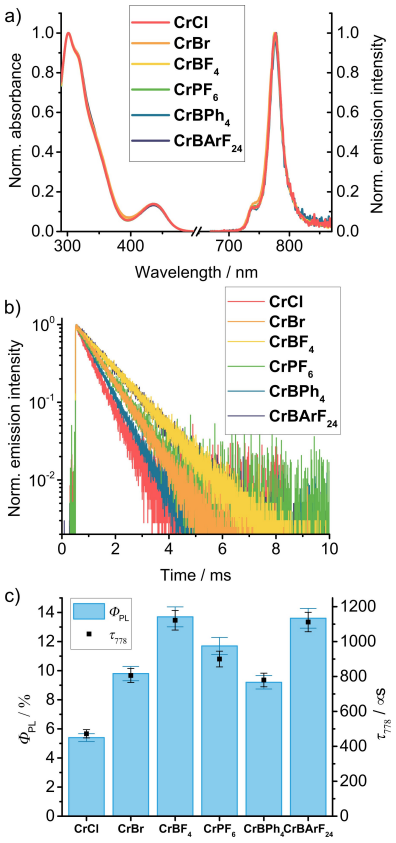

Figure 3. a) Absorption and luminescence emission spectra of $[Cr(ddpd)_2]^{3+}$ with various counter anions in MeCN, b) luminescence decays of the complexes in deaerated MeCN (298 K, $\lambda_{exc.}$ = 435 nm, $\lambda_{em.}$ = 778 nm), and c) bar diagrams of the luminescence quantum yield Φ_{PL} and fitted lifetime τ_{778} of $[Cr(ddpd)_2]^{3+}$ with various counter anions in deaerated MeCN (298 K, λ_{exc} = 435 nm). Relative uncertainties of Φ_{PL} and τ_{778} are estimated to be 5 %.

interactions of the electron rich phenyl groups of the borate anions with the pyridine rings of the ddpd ligands. Consequently, C–H moieties of the borate anions can approach the emissive Cr^{III} center and open additional multiphonon relaxation pathways[12f] which reduce Φ_{PL} and τ_{778}.[18h] To confirm this, spectroscopic studies of **$CrBPh_4$** were performed in deaerated benzonitrile (PhCN). In this aromatic solvent, the complex showed a significantly lower Φ_{PL} of 2.1 ± 0.1 % and a τ_{778} of 83 ± 4 µs in the absence of oxygen compared to the data obtained in deaerated MeCN under the same conditions (SI, Figure S17). This, together with the shortened lifetime of the longer decay component of **$CrBPh_4$** aggregates compared to the Φ_{PL} and τ_{778} of **$CrBF_4$** in pure MeCN solution discussed in the previous section (SI, Figure S16, Table S8), strongly support our hypothesis of enhanced PL quenching via π–π and CH–π stacking. Such an effect can be eliminated by introducing the bulky fluorinated derivative $[BArF_{24}]^-$, as substantiated by the clearly improved Φ_{PL} and τ_{778} of **$CrBArF_{24}$** in MeCN (Figure 3c, Table 3).

Luminescence Properties of $[Cr(ddpd)_2][X]_3$ In Polystyrene Nanoparticles

In the polystyrene matrix of the PSNPs, the counter anions had a negligible influence on the luminescence excitation and emission spectra, regardless of whether the measurements were performed in aqueous suspension or with dried polymer films (SI, Figure S18). A comparison with the results of the solution studies reveals increased Φ_{PL} and τ_{778} for **$CrBF_4$**, **$CrPF_6$**, **$CrBPh_4$**, and **$CrBArF_{24}$** encapsulated in silica-coated PSNPs (same loading concentration of 1 mM used for all particles, see SI) in the presence of oxygen (Figure 4, Table 3). The thin and most likely incomplete silica surface shell, which should be still permeable for O_2, can efficiently protect the $[Cr(ddpd)_2]^{3+}$ from leaking, but is expected to barely affect the PL properties and quenching by oxygen, as shown in a previous study on a temperature, oxygen. and pH sensor.[12h] The only moderate influence of the counter anion under these conditions is ascribed to a combination of the lower oxygen solubility in water (0.29 mM)[30] than in MeCN (1.9 mM;[31] 2.42 mM[31]), the reduced permeability of the polymeric matrix (oxygen permeability coefficient of polystyrene: 1.9×10^{19} $m^2 s^{-1} Pa^{-1}$),[32] and a possible shielding effect of the silica shell.[33]

Sealing the complex-stained PSNPs with an oxygen-barrier film of polyvinyl alcohol (PVOH)[34] led to Φ_{PL} of **$CrBF_4$**, **$CrPF_6$**, **$CrBPh_4$** and **$CrBArF_{24}$** of $11.7\pm0.6\%$, $15.2\pm0.8\%$, $11.3\pm0.6\%$, and $13.4\pm0.7\%$ under air, respectively. Simultaneously, the PL lifetimes increased to values above 900 µs (Table 3). These PL properties are similar or even better than those observed in deaerated PSNP suspension or deaerated MeCN solution under ambient conditions. For **$CrPF_6$** in a PS(Cr)-S-PVOH film, a record Φ_{PL} for non-deuterated $[Cr(ddpd)_2]^{3+}$ of $15.2\pm0.8\%$ was achieved, which is not affected by oxygen.

In summary, in solution, the counter anions and solvent molecules can affect the PL properties of the chromium(III) complexes via different quenching mechanisms, *e.g.* self-quenching caused by chloride ions or ππ stacking. These undesired quenching effects can be efficiently eliminated by introducing bulky counter anions or the incorporation of hydrophobic complexes into an apolar matrix like polystyrene. In the crystalline state, these factors only slightly affect the PL properties. The PL properties of the crystals are mainly governed by the crystal packing, metal···metal distances, and the underlying energy/electron transfer processes.

Oxygen Sensitivity

As shown above, oxygen can quench the phosphorescence of $[Cr(ddpd)_2]^{3+}$. Dexter energy transfer from the excited chromium(III) complex to triplet oxygen yields singlet oxygen $^1O_2$ and the ground state complex.[15] Subsequently, Stern-Volmer studies[35] in the intensity (PL intensity I_{778}) and lifetime domain (lifetime τ_{778}) were performed in MeCN for all six Cr^{III} complex salts and oxygen (Figure 5; SI, Figures S19–S25). The Stern-Volmer constants of all salts derived from intensity $K_{SV}(I)$ and lifetime measurements $K_{SV}(\tau)$ agree within the estimated uncertainties (Table 4), pointing to dynamic quenching in all cases. $K_{SV}(\tau)$ increases in the order of **$CrCl < CrBr < CrBPh_4 < CrPF_6 < CrBF_4 \approx CrBArF_{24}$** with values of $(5.66\pm0.13)\times10^{-2}$ hPa^{-1} to $(12.59\pm0.10)\times10^{-2}$ hPa^{-1} (Figure 5, Table 4). This trend is in line with the lifetimes τ_0 in the absence of oxygen. A longer-lived emissive state has a higher probability for diffusional quenching by oxygen, resulting in a stronger luminescence response, *i.e.*, change in PL (I_0/I or τ_0/τ, *i.e.* a higher K_{SV}) upon a change of the oxygen concentration.[35c,36]

The same trend was also observed for the complex-stained PSNPs (Table 4; SI, Figures S26–S29). Thus, the oxygen sensitivity of $[Cr(ddpd)_2]^{3+}$ could be enhanced by bulky counter anions like *e.g.* $[BArF_{24}]^-$ due to the prolonged τ_0. However, within the stated experimental uncertainties, the counter anions do not affect the oxygen quenching rate constant $k_q = K_{SV}/\tau_0$ of ca. 116 $hPa^{-1}s^{-1}$ on average in solution (Table 4). Consequently, the counter anions have no shielding effect for oxygen quenching in solution. In aqueous PSNP suspension, the k_q values of approximately 15 $hPa^{-1}s^{-1}$ are about one order of magnitude lower than in MeCN solution (Table 4). This is ascribed to a combined effect of some shielding of the particle matrix[33] and the higher viscosity of H_2O compared to MeCN ($\eta(H_2O):\eta(MeCN)\approx2.5$ at 25 °C),[37] which can slow down oxygen diffusion.[35c,36]

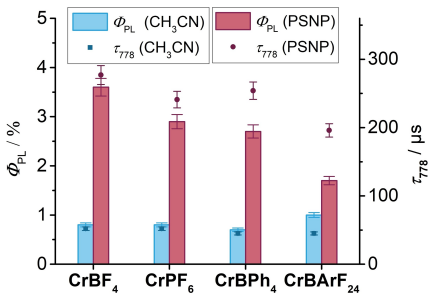

Figure 4. Bar diagrams of Φ_{PL} and τ_{778} of $[Cr(ddpd)_2]^{3+}$ with various counter anions in air-saturated MeCN and aqueous PSNP suspension at 298 K ($\lambda_{exc}=435$ nm, $\lambda_{em}=778$ nm). The relative uncertainties of Φ_{PL} and τ_{778} measurements are estimated to be 5%.

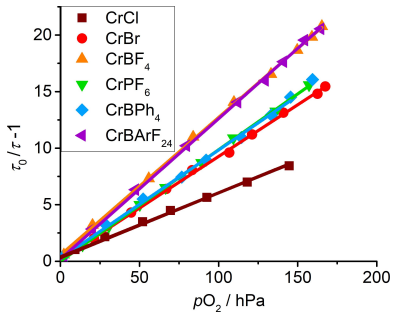

Figure 5. Lifetime-based Stern-Volmer plots of $[Cr(ddpd)_2]^{3+}$ with different counter anions in MeCN in the presence of different oxygen concentrations and the corresponding linear regressions. Lifetime measurements were done with $\lambda_{exc}=435$ nm and $\lambda_{em}=778$ nm, respectively.

Table 4. PL intensity- and lifetime-based Stern-Volmer constants $K_{SV}(I)$ and $K_{SV}(\tau)$ as well as oxygen quenching rate constants k_q of $[Cr(ddpd)_2]^{3+}$ in MeCN (top) obtained in the presence of varying oxygen concentrations and in aqueous suspension of PSNP loaded with these complexes. The corresponding data obtained for aqueous dispersions of PSNP loaded with these complexes are provided as well (bottom).[a]

	CrCl MeCN	**CrBr**	**$CrBF_4$**	**$CrPF_6$**	**$CrBPh_4$**	**$CrBArF_{24}$**
τ_0 [µs]	472 ±24	806 ±40	1122 ±56	900[b] ±45	780 ±39	1112 ±56
$K_{SV}(I)$ [10^{-2} hPa^{-1}]	5.42 ±0.13	8.69 ±0.08	11.96 ±0.34	10.45 ±0.13	9.40 ±0.19	12.37 ±0.10
$K_{SV}(\tau)$ [10^{-2} hPa^{-1}]	5.66 ±0.13	9.13 ±0.09	12.59 ±0.10	9.86 ±0.07	9.60 ±0.18	12.42 ±0.10
k_q [$hPa^{-1}s^{-1}$]	120±7	113±6	112±6	110±6	123±7	112±6
	PS(Cr)-S suspension in water					
τ_0 [µs]			885 ±44	928 ±46	686 ±34	1270[c] ±57
$K_{SV}(I)$ [10^{-2} hPa^{-1}]			1.22 ±0.01	1.44 ±0.05	0.95 ±0.01	1.97 ±0.16
$K_{SV}(\tau)$ [10^{-2} hPa^{-1}]			1.23 ±0.02	1.40 ±0.04	0.96 ±0.03	2.08 ±0.15
k_q [$hPa^{-1}s^{-1}$]			13.9 ±0.7	15.1 ±0.9	14.0 ±0.8	16.4 ±1.4

[a] PS(Cr)-S: PSNPs doped with chromium(III) complexes and coated with a thin silica shell. Measurements of τ_0 were done in deaerated MeCN or aqueous water suspension with λ_{exc} = 435 nm and λ_{em} = 778 nm. The relative uncertainty of the τ_{778} values is estimated to be 5%. The errors of the fitted K_{SV} and calculated k_q are given in the table. [b] Φ_{PL} and τ_{778} are cited from Ref. [12b]. [c] The luminescence decay was fitted biexponentially and the averaged lifetimes were calculated from amplitude weighted fits.

Conclusion and Outlook

In summary, the photophysical properties of oxygen-sensitive $[Cr(ddpd)_2]^{3+}$ complexes with six different counter anions, ranging from simple halide ions to bulky borate anions, were systematically investigated in the crystalline state, in acetonitrile (MeCN) solution, in polystyrene nanoparticles (PSNP), and in poly(vinyl alcohol) coated films of these nanoparticles. Contrary to the reduced self-quenching of typical charge-transfer emitters such as Ir^{III} complexes by large counter ions,[19] the metal-centered nature of the excited states of $[Cr(ddpd)_2]^{3+}$ renders its excited state properties less dependent on the counter ion. In single crystals of various salts, photoluminescence quantum yields varied between 4.5 and 13.7%. In MeCN solution, only tetraphenyl borate and high chloride concentrations quench the photoluminescence (PL) of the emissive doublet states $^2E/^2T_1$ of chromium(III) by multiphonon relaxation and self-quenching, respectively. In the case of the bromide salt, the reduced luminescence quantum yield is attributed to photoinduced electron transfer (PET) or enhanced intersystem crossing (ISC) to the ground state.

In deaerated MeCN solutions and in PSNP suspensions, Φ_{PL} and τ_{778} of the chromium(III) complexes are improved by bulky anions, *e.g.* $[BArF_{24}]^-$, while the involved energy levels remained unaffected. Consequently, the oxygen sensitivity is enhanced with bulky anions. The microsecond-scale lifetimes and the high PL response to oxygen suggest their application potential for time-resolved biosensing.[38] Interestingly, the $[BF_4]^-$ salt gave very high values for lifetime and quantum yield similar to those of the $[BArF_{24}]^-$ salt.

The positive correlation between the PL quantum yields and the PL lifetimes of the six $[Cr(ddpd)_2]^{3+}$ complex salts shows that the surroundings hardly affect the intersystem crossing rate[15] from the initially excited $^4T_2$ state to the emissive $^2E/^2T_1$ states. Instead, they influence the radiative and non-radiative deactivation pathways to the ground state ($^2E/^2T_1 \rightarrow {}^4A_2$).

Encapsulating the $[PF_6]^-$ salt in PSNP and embedding these nanoparticles in oxygen-shielding poly(vinyl alcohol) yielded an oxygen insensitive NIR-emitting polymer film that exhibits a PL quantum yield of 15.2% with a near millisecond luminescence lifetime, which is a promising label for bioimaging studies.[38]

Experimental Section

Experimental synthetic and spectroscopic details can be found in the Supporting Information.

Acknowledgements

The authors acknowledge Dr. Luca M. Carella and Dr. Dieter Schollmeyer for XRD measurements and thank Dimitri Zorn and Florian Reichenauer for their valuable support of the optimized ligand synthesis. This work was supported by the Deutsche Forschungsgemeinschaft (RE 1203/23-1, HE 2778/10-1). W. R. K. is grateful for a Kekulé scholarship of the Fonds der Chemischen Industrie (FCI). Open Access funding enabled and organized by Projekt DEAL.

Conflict of Interest

The authors declare no conflict of interest.

Data Availability Statement

The data that support the findings of this study are available from the corresponding author upon reasonable request.

Keywords: chromium · counter anions · photoluminescence · oxygen quenching · second coordination sphere

[1] M. K. Nazeeruddin, M. Grätzel in *Transition Metal Complexes for Photovoltaic and Light Emitting Applications*, (Ed. V. W. W. Yam), Springer, Berlin, Heidelberg, **2007**, pp. 113–175.
[2] a) Q. Zhao, C. Huang, F. Li, *Chem. Soc. Rev.* **2011**, *40*, 2508–2524; b) D. L. Ma, H. Z. He, K. H. Leung, D. S. Chan, C. H. Leung, *Angew. Chem. Int. Ed.* **2013**, *52*, 7666–7682; *Angew. Chem.* **2013**, *125*, 7820–7837.
[3] J. Twilton, C. Le, P. Zhang, M. H. Shaw, R. W. Evans, D. W. C. MacMillan, *Nat. Chem. Rev.* **2017**, *1*, 0052.
[4] R. D. Costa, E. Orti, H. J. Bolink, F. Monti, G. Accorsi, N. Armaroli, *Angew. Chem. Int. Ed.* **2012**, *51*, 8178–8211; *Angew. Chem.* **2012**, *124*, 8300–8334.
[5] a) K. K.-W. Lo, S. P.-Y. Li, *RSC Adv.* **2014**, *4*, 10560; b) S. M. Borisov, G. Zenkl, I. Klimant, *ACS Appl. Mater. Interfaces* **2010**, *2*, 366–374; c) I. M. Dixon, E. Lebon, P. Sutra, A. Igau, *Chem. Soc. Rev.* **2009**, *38*, 1621–1634 ; d) M. de Barros e Silva Botelho, J. M. Fernandez-Hernandez, T. B. de Queiroz, H. Eckert, L. De Cola, A. S. S. de Camargo, *J. Mater. Chem.* **2011**, *21*, 8829; e) C. Wei, L. Ma, H. Wei, Z. Liu, Z. Bian, C. Huang, *Sci. China Technol. Sci.* **2018**, *61*, 1265–1285.
[6] a) A. Hossain, A. Bhattacharyya, O. Reiser, *Science* **2019**, *364*, eaav9713; b) M. Gernert, L. Balles-Wolf, F. Kerner, U. Muller, A. Schmiedel, M. Holzapfel, C. M. Marian, J. Pflaum, C. Lambert, A. Steffen, *J. Am. Chem. Soc.* **2020**, *142*, 8897–8909; c) T. Brandl, C. Kerzig, L. Le Pleux, A. Prescimone, O. S. Wenger, M. Mayor, *Chem. Eur. J.* **2020**, *26*, 3119–3128.
[7] a) Y. Zhang, T. S. Lee, J. M. Favale, D. C. Leary, J. L. Petersen, G. D. Scholes, F. N. Castellano, C. Milsmann, *Nat. Chem.* **2020**, *12*, 345–352; b) M. Yang, S. Sheykhi, Y. Zhang, C. Milsmann, F. N. Castellano, *Chem. Sci.* **2021**, *12*, 9069–9077.
[8] a) K. S. Kjær, N. Kaul, O. Prakash, P. Chábera, N. W. Rosemann, A. Honarfar, O. Gordivska, L. A. Fredin, K.-E. Bergquist, L. Häggström, T. Ericsson, L. Lindh, A. Yartsev, S. Styring, P. Huang, J. Uhlig, J. Bendix, D. Strand, V. Sundström, P. Persson, R. Lomoth, K. Wärnmark, *Science* **2019**, *363*, 249–253; b) A. K. Mengel, C. Förster, A. Breivogel, K. Mack, J. R. Ochsmann, F. Laquai, V. Ksenofontov, K. Heinze, *Chem. Eur. J.* **2015**, *21*, 704–714; c) O. S. Wenger, *Chem. Eur. J.* **2019**, *25*, 6043–6052; d) G. Bauer, X. Hu, *Inorg. Chem. Front.* **2016**, *3*, 741–765; e) P. Dierks, Y. Vukadinovic, M. Bauer, *Inorg. Chem. Front.* **2022**, *9*, 206–220; f) W. Leis, M. A. Arguello Cordero, S. Lochbrunner, H. Schubert, A. Berkefeld, *J. Am. Chem. Soc.* **2022**, *144*, 1169–1173.
[9] a) L. A. Büldt, X. Guo, A. Prescimone, O. S. Wenger, *Angew. Chem. Int. Ed.* **2016**, *55*, 11247–11250; *Angew. Chem.* **2016**, *128*, 11413–11417; b) P. Herr, F. Glaser, L. A. Büldt, C. B. Larsen, O. S. Wenger, *J. Am. Chem. Soc.* **2019**, *141*, 14394–14402; c) P. Herr, O. S. Wenger, *Inorganics* **2020**, *8*, 14; d) P. Boden, P. Di Martino-Fumo, T. Bens, S. Steiger, U. Albold, G. Niedner-Schatteburg, M. Gerhards, B. Sarkar, *Chem. Eur. J.* **2021**, *27*, 12959–12964.
[10] a) P. Herr, C. Kerzig, C. B. Larsen, D. Häussinger, O. S. Wenger, *Nat. Chem.* **2021**, *13*, 956–962; b) K. Heinze, *Nat. Chem.* **2021**, *13*, 926–928.
[11] a) A. K. Pal, C. Li, G. S. Hanan, E. Zysman-Colman, *Angew. Chem. Int. Ed.* **2018**, *57*, 8027–8031; *Angew. Chem.* **2018**, *130*, 8159–8163; b) S. Kaufhold, N. W. Rosemann, P. Chabera, L. Lindh, I. Bolano Losada, J. Uhlig, T. Pascher, D. Strand, K. Warnmark, A. Yartsev, P. Persson, *J. Am. Chem. Soc.* **2021**, *143*, 1307–1312.
[12] a) L. A. Büldt, X. Guo, R. Vogel, A. Prescimone, O. S. Wenger, *J. Am. Chem. Soc.* **2017**, *139*, 985–992; b) S. Otto, M. Grabolle, C. Förster, C. Kreitner, U. Resch-Genger, K. Heinze, *Angew. Chem. Int. Ed.* **2015**, *54*, 11572–11576; *Angew. Chem.* **2015**, *127*, 11735–11739; c) U. Basu, S. Otto, K. Heinze, G. Gasser, *Eur. J. Inorg. Chem.* **2019**, 37–41; d) S. Otto, C. Förster, C. Wang, U. Resch-Genger, K. Heinze, *Chem. Eur. J.* **2018**, *24*, 12555–12563; e) S. Otto, J. P. Harris, K. Heinze, C. Reber, *Angew. Chem. Int. Ed.* **2018**, *57*, 11069–11073; *Angew. Chem.* **2018**, *130*, 11236–11240; f) C. Wang, S. Otto, M. Dorn, E. Kreidt, J. Lebon, L. Srsan, P. Di Martino-Fumo, M. Gerhards, U. Resch-Genger, M. Seitz, K. Heinze, *Angew. Chem. Int. Ed.* **2018**, *57*, 1112–1116; *Angew. Chem.* **2018**, *130*, 1125–1130; g) S. Otto, M. Dorn, C. Förster, M. Bauer, M. Seitz, K. Heinze, *Coord. Chem. Rev.* **2018**, *359*, 102–111; h) C. Wang, S. Otto, M. Dorn, K. Heinze, U. Resch-Genger, *Anal. Chem.* **2019**, *91*, 2337–2344; i) J. Kalmbach, C. Wang, Y. You, C. Förster, H. Schubert, K. Heinze, U. Resch-Genger, M. Seitz, *Angew. Chem. Int. Ed.* **2020**, *59*, 18804–18808; *Angew. Chem.* **2020**, *132*, 18966–18970; j) S. Treiling, C. Wang, C. Förster, F. Reichenauer, J. Kalmbach, P. Boden, J. P. Harris, L. M. Carrella, E. Rentschler, U. Resch-Genger, C. Reber, M. Seitz, M. Gerhards, K. Heinze, *Angew. Chem. Int. Ed.* **2019**, *58*, 18075–18085; *Angew. Chem.* **2019**, *131*, 18243–18253; k) F. Reichenauer, C. Wang, C. Förster, P. Boden, N. Ugur, R. Báez-Cruz, J. Kalmbach, L. M. Carrella, E. Rentschler, C. Ramanan, G. Niedner-Schatteburg, M. Gerhards, M. Seitz, U. Resch-Genger, K. Heinze, *J. Am. Chem. Soc.* **2021**, *143*, 11843–11855; l) S. Otto, N. Scholz, T. Behnke, U. Resch-Genger, K. Heinze, *Chem. Eur. J.* **2017**, *23*, 12131–12135; m) N. Sinha, J. R. Jimenez, B. Pfund, A. Prescimone, C. Piguet, O. S. Wenger, *Angew. Chem. Int. Ed.* **2021**, *60*, 23722–23728.
[13] a) C. Förster, K. Heinze, *Chem. Soc. Rev.* **2020**, *49*, 1057–1070; b) C. B. Larsen, O. S. Wenger, *Chem. Eur. J.* **2018**, *24*, 2039–2058; c) O. S. Wenger, *J. Am. Chem. Soc.* **2018**, *140*, 13522–13533.
[14] a) A. D. Kirk, *Chem. Rev.* **1999**, *99*, 1607–1640; b) L. S. Forster, *Coord. Chem. Rev.* **2002**, *227*, 59–92; c) N. A. P. Kane-Maguire, *Top. Curr. Chem.* **2007**, *280*, 37–67; d) V. Balzani, P. Ceroni,A. Juris, *Photochemistry and Photophysics*, Wiley-VCH, Weinheim, **2014**, p. 216; e) C. K. Ryu, J. F. Endicott, *Inorg. Chem.* **1988**, *27*, 2203–2214; f) T. H. Maiman, *Nature* **1960**, *187*, 493; g) M. A. Jamieson, N. Serpone, M. Z. Hoffman, *Coord. Chem. Rev.* **1981**, *39*, 121–179; h) C. Wegeberg, O. S. Wenger, *JACS Au* **2021**, *1*, 1860–1876; i) M. Poncet, A. Benchohra, J. R. Jiménez, C. Piguet, *ChemPhotoChem* **2021**, *5*, 880–892.
[15] S. Otto, A. M. Nauth, E. Ermilov, N. Scholz, A. Friedrich, U. Resch-Genger, S. Lochbrunner, T. Opatz, K. Heinze, *ChemPhotoChem* **2017**, *1*, 344–349.
[16] a) C. Dee, F. Zinna, W. R. Kitzmann, G. Pescitelli, K. Heinze, L. Di Bari, M. Seitz, *Chem. Commun.* **2019**, *55*, 13078–13081; b) J.-R. Jiménez, B. Doistau, C. M. Cruz, C. Besnard, J. M. Cuerva, A. G. Campaña, C. Piguet, *J. Am. Chem. Soc.* **2019**, *141*, 13244–13252; c) J.-R. Jiménez, M. Poncet, S. Miguez-Lago, S. Grass, J. Lacour, C. Besnard, J. M. Cuerva, A. G. Campana, C. Piguet, *Angew. Chem. Int. Ed.* **2021**, *60*, 10095–10102.
[17] J.-R. Jiménez, B. Doistau, C. Besnard, C. Piguet, *Chem. Commun.* **2018**, *54*, 13228–13231.
[18] a) Y. Zhu, Y. Ma, J. Zhu, *J. Lumin.* **2013**, *137*, 198–203; b) G. H. Eom, J. H. Kim, Y. D. Jo, E. Y. Kim, J. M. Bae, C. Kim, S.-J. Kim, Y. Kim, *Inorg. Chim. Acta* **2012**, *387*, 106–116; c) M. Pan, M.-H. Lan, X.-T. Wang, C. Yan, Y. Liu, C.-Y. Su, *Inorg. Chim. Acta* **2010**, *363*, 3757–3764; d) T. Gneuss, M. J. Leitl, L. H. Finger, H. Yersin, J. Sundermeyer, *Dalton Trans.* **2015**, *44*, 20045–20055; e) D. Ma, C. Zhang, Y. Qiu, L. Duan, *Org. Electron.* **2016**, *39*, 16–24; f) R. Mondal, I. B. Lozada, R. L. Davis, J. A. G. Williams, D. E. Herbert, *J. Mater. Chem. C* **2019**, *7*, 3772–3778; g) Y. Ma, Y. Dong, P. She, S. Liu, M. Xie, Y. Yu, Y. Li, Q. Zhao, W. Huang, *Adv. Opt. Mater.* **2018**, *6*, 1801065; h) M. Martínez-Alonso, P. Sanz, P. Ortega, G. Espino, F. A. Jalón, M. Martín, A. M. Rodríguez, J. A. López, C. Tejel, B. R. Manzano, *Inorg. Chem.* **2020**, *59*, 14171–14183; i) E. P. Farney, S. J. Chapman, W. B. Swords, M. D. Torelli, R. J. Hamers, T. P. Yoon, *J. Am. Chem. Soc.* **2019**, *141*, 6385–6391.
[19] D. Ma, L. Duan, Y. Wei, L. He, L. Wang, Y. Qiu, *Chem. Commun.* **2014**, *50*, 530–532.
[20] A. Breivogel, C. Förster, K. Heinze, *Inorg. Chem.* **2010**, *49*, 7052–7056.
[21] T. Behnke, C. Würth, E.-M. Laux, K. Hoffmann, U. Resch-Genger, *Dyes Pigm.* **2012**, *94*, 247–257.
[22] a) W. Stöber, A. Fink, E. Bohn, *J. Colloid Interface Sci.* **1968**, *26*, 62–69; b) A. Van Blaaderen, J. Van Geest, A. Vrij, *J. Colloid Interface Sci.* **1992**, *154*, 481–501.
[23] D. E. Chandler, Z. K. Majumdar, G. J. Heiss, R. M. Clegg, *J. Fluoresc.* **2006**, *16*, 793–807.
[24] a) D. L. Dexter, *J. Chem. Phys.* **1953**, *21*, 836–850; b) S. Speiser, *Chem. Rev.* **1996**, *96*, 1953–1976.
[25] E. Previtera, A. Tissot, A. Hauser, *Eur. J. Inorg. Chem.* **2016**, *2016*, 1972–1979.
[26] a) L. Troian-Gautier, M. D. Turlington, S. A. M. Wehlin, A. B. Maurer, M. D. Brady, W. B. Swords, G. J. Meyer, *Chem. Rev.* **2019**, *119*, 4628–4683; b) G. Li, W. M. Ward, G. J. Meyer, *J. Am. Chem. Soc.* **2015**, *137*, 8321–8323; c) G. Li, M. D. Brady, G. J. Meyer, *J. Am. Chem. Soc.* **2018**, *140*, 5447–5456; d) G. Li, W. B. Swords, G. J. Meyer, *J. Am. Chem. Soc.* **2017**, *139*, 14983–14991.
[27] a) N. G. Connelly, W. E. Geiger, *Chem. Rev.* **1996**, *96*, 877–910; b) D. M. Stanbury in *Reduction Potentials Involving Inorganic Free Radicals in*

Aqueous Solution, Vol. 33 (Ed. A. G. Sykes), Elsevier, New York, **1989**, pp. 69–138.
[28] a) S. P. McGlynn, J. Daigre, F. J. Smith, *J. Chem. Phys.* **1963**, *39*, 675–679; b) X. Sun, B. Zhang, X. Li, C. O. Trindle, G. Zhang, *J. Phys. Chem. A* **2016**, *120*, 5791–5797.
[29] R. Sriram, M. Z. Hoffman, M. A. Jamieson, N. Serpone, *J. Am. Chem. Soc.* **1980**, *102*, 1754–1756.
[30] M. Montalti, A. Credi, L. Prodi, M. T. Gandolfi, *Handbook of Photochemistry*, CRC Taylor & Francis, Boca Raton, FL, **2006**.
[31] C. Fano, J. Olmstedt III, *Talanta* **1990**, *37*, 905–909.
[32] C. Courgneau, S. Domenek, A. Guinault, L. Avérous, V. Ducruet, *J. Polym. Environ.* **2011**, *19*, 362–371.
[33] O. S. Kwon, J. H. Kim, J. K. Cho, J. H. Kim, *ACS Appl. Mater. Interfaces* **2015**, *7*, 318–325.
[34] J. Gaume, P. Wong-Wah-Chung, A. Rivaton, S. Thérias, J.-L. Gardette, *RSC Adv.* **2011**, *1*, 1471–1481.
[35] a) O. Stern, M. Volmer, *Z. Phys.* **1919**, *20*, 183–188; b) H. Boaz, G. K. Rollefson, *J. Am. Chem. Soc.* **1950**, *72*, 3435–3443; c) M. H. Gehlen, *J. Photochem. Photobiol. C* **2020**, *42*, 100338.
[36] M. Arık, N. Celebi, Y. Onganer, *J. Photochem. Photobiol. A* **2005**, *170*, 105–111.
[37] a) L. Korson, W. Drost-Hansen, F. J. Millero, *J. Phys. Chem.* **1969**, *71*, 34–39; b) G. Rltzoulls, N. Papadopoulos, D. Jannakoudakls, *J. Chem. Eng. Data* **1986**, *31*, 146–148.
[38] a) Q. Wu, P. Dai, Y. Wang, J. Zhang, M. Li, K. Y. Zhang, S. Liu, W. Huang, Q. Zhao, *Chem. Sci.* **2021**, *12*, 11020–11027; b) Y. Ning, G. Q. Jin, M. X. Wang, S. Gao, J. L. Zhang, *Curr. Opin. Chem. Biol.* **2021**, *66*, 102097.
[39] Deposition Number(s) 2121328 (**CrCl**×3 EtOH×H_2O), 2121329 (**CrCl**×2 EtOH×3 H_2O), 2121330 (**CrCl**×3.5 MeOH×0.5 NH_4Cl), 2121331 (CrBr×3 H_2O×MeCN), 2121332 (**CrCl**×2 MeOH×4 H_2O), 2121333 (**$CrPF_6$**×3 MeCN) contain(s) the supplementary crystallographic data for this paper. These data are provided free of charge by the joint Cambridge Crystallographic Data Centre and Fachinformationszentrum Karlsruhe Access Structures service www.ccdc.cam.ac.uk/structures.

Manuscript received: December 22, 2021
Revised manuscript received: February 7, 2022
Accepted manuscript online: February 21, 2022
Version of record online: March 18, 2022